MCB Accepted Manuscript Posted Online 12 December 2016
Mol. Cell. Biol. doi:10.1128/MCB.00522-16

The chromatin associated Phf12 protein maintains nucleolar integrity and prevents premature cellular senescence.

Running Title: Pf1 regulates ribosomal biogenesis

Richard Graveline [1, #], Katarzyna Marcinkiewicz [1, #], Seyun Choi [1], Marilène Paquet [2], Wolfgang Wurst [3], Thomas Floss [3], and Gregory David [1, *]

1. New York University School of Medicine, New York, NY, United States.
2. Faculté de Médecine Vétérinaire, Université de Montréal, Saint-Hyacinthe (Québec), Canada
3. Helmholtz Zentrum München - German Research Center for Environmental Health, Neuherberg, Germany

# Contributed equally

***CORRESPONDENCE**: Gregory David
Dept. of Biochemistry and Molecular Pharmacology, MSB417
NYU Langone Medical Center
550 First Ave.
New York, NY10016.
gregory.david@nyumc.org
Ph: 212-263-2926; Fax: 212-263-7133

KEYWORDS: Transcription; Ribosome; Pf1; Senescence; Nucleolus

Abstract

PF1, also known as PHF12 (plant homeodomain (PHD) zinc finger protein 12) is a member of the PHD zinc finger family of proteins. PF1 associates with a chromatin interacting protein complex comprised of MRG15, Sin3B, and HDAC1, that functions as a transcriptional modulator. The biological function of Pf1 remains largely elusive. We undertook the generation of *Pf1* knockout mice to elucidate its physiological role. We demonstrate that *Pf1* is required for mid-to-late gestation viability. *Pf1* inactivation impairs the proliferative potential of the mouse embryonic fibroblasts (MEFs), and is associated with a significant decrease in BrdU incorporation, an increase in SA-β-gal activity, a marker of cellular senescence and elevated levels of phosphorylated H2AX (γ-H2AX), a marker associated with DNA double-strand breaks. Analysis of transcripts differentially expressed in wild-type and Pf1 deficient cells reveals the impact of Pf1 in multiple regulatory arms of the ribosome biogenesis pathways. Strikingly, assessing the morphology of the nucleoli exposes abnormal nucleolar structure in Pf1 deficient cells. Finally, proteomic analysis of the Pf1-interacting complexes highlighted proteins involved in ribosome biogenesis. Taken together, our data reveal an unsuspected function for the Pf1-associated chromatin complex in the ribosomal biogenesis and senescence pathways.

43 **Introduction**

44 Pf1, also known as Phf12 (plant homeodomain (PHD) zinc finger protein 12) is a member
45 of the PHD zinc finger family of proteins. PHD domains are small, 50 to 80 aminoacids long
46 domains, often found in clusters of two or three and/or in proximity of other chromatin
47 interacting domains, such as bromo-or chromodomains. Consistently, many of the PHD
48 containing proteins are nuclear proteins that interact with chromatin. Increasing evidence
49 suggest that PHD domains are capable of recognizing modified and un-modified histone
50 tails, and that PHD domain-containing proteins act as epigenetic readers (1).

51 The *Pf1* gene is conserved throughout evolution and the Pf1 protein, like its yeast homolog
52 Rco1, contains two PHD domains in its N-terminus. Mammalian Pf1 was first identified in a
53 yeast-two hybrid screen for proteins interacting with the paired amphipathic helix (PAH) 2
54 domain of Sin3A, and shown to function as a transcriptional repressor (2). A later report
55 identified Pf1 as one of the components of human MRG15 complex, together with SIN3B,
56 but not with its close homolog SIN3A (3). The PHD domains of PF1 are important for the
57 interaction with the MRG domain of MRG15, which relies mainly on hydrophobic
58 interactions (3-5). The interaction of PF1 with a complex containing SIN3B, and not SIN3A,
59 was also confirmed in experiments identifying associations between SIN3B, the histone
60 deacetylase HDAC1, MRG15, and PF1. While its precise function in transcriptional
61 regulation remains unclear, the PF1-MRG15-SIN3B-HDAC complex appears to modulate
62 RNAPII progression at actively transcribed regions, similar to what has been reported for
63 the Rpd3S complex, its yeast homolog (6).

64 Reports assessing the biological function of Pf1 point to roles in phosphoinositide signaling
65 (7), nervous system development (8), and epithelial to mesenchymal transition and
66 maintenance of a stem cell phenotype (9). To our knowledge, no comprehensive study
67 elucidating the in vivo function of Pf1 protein has been conducted so far.

68 Mouse strains with genetic inactivation of Sin3B, HDAC1, or MRG15, the three components
69 of the protein complex repeatedly shown to also contain the Pf1 protein, have previously
70 been described. The Sin3B-/- embryos reveal global retardation in size, pale color,

71 abnormal hematopoietic picture in the liver, and reduction in bone deposition at later
72 embryonic stages, and die shortly before birth (10). Sin3B knockout mouse embryonic
73 fibroblasts (MEFs) are refractory to quiescence and to oncogene-induced senescence (OIS),
74 a stable cell-cycle arrest in response to oncogene activation (10-13). Knockout of HDAC1
75 leads to embryonic lethality before day 10.5 of gestation, and HDAC1-/- embryos examined
76 at earlier embryonic stages are extremely growth retarded as a result of a defect in cell
77 proliferation (14, 15). Loss of HDAC1 in ES cells leads to impaired proliferation that is
78 associated with up-regulated expression of CDK inhibitors p21 and p27 (14), but
79 conditional HDAC1 knockout in MEFs does not affect the cell proliferation under normal
80 conditions (16). Similarly, genetic inactivation of MRG15 results in embryonic lethality
81 between embryonic day 14.5 (E14.5) and birth. The null embryos are smaller than wild-
82 type and heterozygous embryos, with most prominent defects in the heart, lung, liver and
83 the keratinocyte-epidermal layer of the skin. The growth potential of Mrg15−/− mouse
84 embryonic fibroblasts (MEFs) is greatly reduced (17).

85 Here, we describe the generation of *Pf1* knockout mice to define the physiological role of
86 Pf1. We report that *Pf1* inactivation leads to embryonic lethality. Moreover, we show that
87 *Pf1* inactivation impairs the proliferative potential of the cells and is associated with a
88 strong nucleolar stress. Taken together, our data demonstrate that Pf1 is crucial for
89 embryogenesis and nuclear functions.

90

91

92 **Methods**

93 **Generation of a Pf1-KO mouse line**

94 The Pf1 -/- mice were derived using the gene- trapping technique. Briefly, this included the
95 identification of the embryonic stem (ES) cell clone with a ROSA26geo cassette integrated
96 into the intron between exons 2 and 3 of the *Pf1* locus, subsequent microinjection of the
97 selected ES cells into blastocysts to generate chimeric mice, and derivation of Pf1 +/- mice.
98 The heterozygous animals were intercrossed, and embryos were collected at different time
99 points.

100 **Histology and IHC**

101 Mouse embryos were fixed overnight in 10% formalin (Thermo Fisher Scientific, Waltham,
102 MA) and processed for paraffin embedding. For histology, deparaffinized sections (5 μm)
103 were stained with Gill's hematoxylin (Richard-Allan Scientific) and eosin Y followed by an
104 alcohol dehydration series and mounting (Permount; Thermo Fisher Scientific, Waltham,
105 MA). Trichrome staining was performed at the NYU School of Medicine Histopathology
106 Core Facility. Paraformaldehyde-fixed, paraffin-embedded, 4-μm sections of tissue were
107 stained using unconjugated polyclonal rabbit anti-mouse Cleaved Caspase-3 (asp-175)
108 (Cell Signaling Technology Cat# 9661S Lot# 42 RRID:AB_331440), and nconjugated rabbit
109 anti-mouse Ki67 clone SP7 (Lab Vision Cat# RM-9106 Lot# 1308g RRID:AB_2335745).

110 **Mouse embryonic fibroblasts (MEFs) isolation, cells and reagents**

111 MEFs were generated from 13.5 and 14.5 days post-coitus embryos. The head and the red
112 organs were removed, and used for genotyping. The torso was then minced and dispersed
113 in 0.1% trypsin (45 min at 37°C). Cells were subsequently grown in DMEM medium
114 supplemented with 10% Fetal Bovine Serum (FBS, Atlanta Biologicals, Flowery Branch,
115 GA), 50 μM β-mercaptoethanol (Sigma Aldrich, St. Louis, MO), and penicillin-streptomycin
116 and sub-cultured 1:4 upon confluency. The cultures were maintained in 6% O2, 5% CO2 at
117 37°C.

118 HeLa S3 cell line was maintained in SMEM medium supplemented with 10% Fetal Bovine
119 Serum, 2mM Glutamine (Corning Inc., Corning, NY), 1% Non Essential Amino Acids (NEAA,
120 Corning Inc., Corning, NY). The cultures were maintained in spinner flasks at 3-
121 $9x10^5$cells/ml, 5% CO2 at 37°C.

122 293T cells were cultured in DMEM medium supplemented with 10% Donor Calf Serum
123 (DCS, Atlanta Biologicals, Flowery Branch, GA) and penicillin-streptomycin (Corning Inc.,
124 Corning, NY) and sub-cultured 1:4 upon confluency. The cultures were maintained in 5%
125 CO2 at 37°C. 293T cells were transfected using a standard calcium phosphate transfection
126 protocol. Viral particles produced were collected for three consecutive days as a
127 suspension in cell medium. Virus suspension was filtered through a Millex-HV Syringe
128 Filter Unit, 0.45 µm (Millipore-Merck KGaA, Darmstadt, Germany), supplemented with 6
129 µg/ml polybrene (Millipore-Merck KGaA, Darmstadt, Germany) and used to infect the HeLa
130 S3 cells.

131 **3T3 protocol/Growth curve**

132 Growth curve experiments were performed essentially as described (18). Briefly, twenty-
133 five thousand cells per well were plated into 12-well plates. At the indicated times, cells
134 were washed with PBS, fixed in 10% formalin, and rinsed with distilled water. Cells were
135 stained with 0.1% crystal violet (Sigma Aldrich, St. Louis, MO) for 30 min, rinsed
136 extensively, and dried. Cell-associated dye was extracted with 2.0 ml 10% acetic acid.
137 Aliquots were diluted 1:4 with H2O, transferred to 96-well microtiter plates, and the
138 optical density at 590 nm was determined. Values were normalized to the optical density at
139 day 0 for the appropriate cell type. Within an experiment, each point was determined in
140 triplicate; each growth curve was performed at least twice.

141 **Gene expression microarray analysis and qPCR**

142 Total RNA from Pf+/+ and Pf1 -/- MEFs at passage 2-3 (Pf+/+ lines 7706-5 and 7706-6
143 and Pf1 -/- lines 7706-2 and 7706-4) was isolated using Trizol reagent (Thermo Fisher
144 Scientific, Waltham, MA) according to the manufacturers protocol. The RNA samples were
145 examined on Affymetrix GeneChip Mouse Genome 430A 2.0 Array (Affymetrix, Santa Clara,

146 CA). Data were analyzed using GenePattern software (19) and DAVID (Database for
147 Annotation, Visualization and Discovery) tools (20, 21). cDNA was synthesized using
148 Moloney Murine Leukemia Virus Reverse Transcriptase (M-MLV RT, Promega, Madison,
149 WI) and quantitative RT-PCR analyses were performed using the Maxima™ SYBR™
150 Green/ROX 2X qPCR Master Mix (Thermo Fisher Scientific, Waltham, MA), following
151 optimized manufacturer's protocols. The raw data from the microarray experiment have
152 been deposited in the GEO database with the GEO accession number GSE86398.

153 **BrdU incorporation**

154 Subconfluent cultures were labeled for 2 hr with 30 μM bromo-deoxyuridine (BrdU;
155 Amersham). Cells were detached with trypsin, fixed in 4% paraformaldehyde, and treated
156 as follows (PBS washes between each step): 4N HCl for 10 minutes at room temperature,
157 0.1M borate (pH 8.5) for 2 min at room temperature; and, finally, permeabilized with 0.1%
158 Triton/3%BSA/PBST for 5min. After subsequent washing steps in PBS-T, cells were then
159 incubated with BrdU antibody (dilution 1:100 in PBS-T) for 80 min and then with an FITC-
160 conjugated secondary antibody (dilution 1:500 in PBS-T, CalBiochem- Merck KGaA,
161 Darmstadt, Germany). Cells were counterstained with DAPI to identify all nuclei, and the
162 percentage of BrdU-labeled cells (FITC/DAPI) was quantified using a fluorescence
163 microscope. At least 200 cells were counted per sample; each experiment was performed at
164 least three times.

165 **SA-β-galactosidase assay**

166 Cells were washed in PBS, fixed for 3-5 min (room temperature) in 3% formaldehyde,
167 washed, and incubated at 37°C with fresh X-gal solution: 1X citric buffer (25 mM Na2HPO4;
168 7.4 mM citric acid; pH 6.0); 150 mM NaCl; 2 mM MgCl2; 5 mM Potassium Ferricyanide; 5
169 mM Potassium Ferrocyanide; 1mg/mL X-gal. Cells were incubating at 37°C overnight. The
170 percentage of SA-β-galactosidase-positive cells was quantified using a phase-contrast
171 inverted microscope. At least 200 cells were counted per sample; each experiment was
172 performed at least three times.

173 **Immunofluorescence**

174 Cells were grown on coverslips to sub-confluence, washed with PBS and fixed in 3%
175 paraformaldehyde/PBS for 10 min at room temperature. Fixed cells were permeabilized
176 with Triton X-100 buffer (0.1% Triton X-100, 20 mM HEPES-KOH pH 7.9, 50 mM NaCl, 3
177 mM MgCl2, 300 mM sucrose) for 5 min and blocked in 0.5% (w/v) BSA (Bovine Serum
178 Albumin, Thermo Fisher Scientific, Waltham, MA) in PBS for 30 min at room temperature.
179 Cells were then incubated with primary antibody in 0.5% (w/v) BSA in PBS for 2 h at room
180 temperature, followed by three 5 min washes with PBS. Fluorescently labeled secondary
181 antibodies in PBS were then added for 1 h at room temperature and coverslips were
182 washed 3x with PBS. Primary antibodies used were: anti γH2A.X (Upstate, no 05-636,
183 Millipore-Merck KGaA, Darmstadt, Germany); anti fibrillarin (Cell Signaling, Danvers, MA,
184 no 2639S); anti UBF (Santa Cruz Biotechnology, Inc. Dallas, TX, sc-9131), anti SENP3 (Cell
185 Signaling, Danvers, MA, no 5591S). The cells were counterstained with TO-PRO3 (Thermo
186 Fisher Scientific, Waltham, MA) following the manufacturer's protocol, and visualized by
187 confocal microscopy.

188 **Co-immunoprecipitation and LC-MS/MS**

189 Transfections and co-immunoprecipitations were performed essentially as described
190 previously (6), using EZview™ Red ANTI-FLAG® M2 Affinity Gel (Sigma Aldrich, St. Louis,
191 MO) during the overnight incubation step. Constructs of Pf1 wt and mutant proteins were
192 generated in our lab. The tagged constructs of APC6, APC7, APC8 used in the co-
193 immunoprecipitation experiments were obtained from Dr. Izawa (Cambridge, UK). PELP1,
194 LAS1L, NPM1 plasmids were a gift from Dr. Muller (Frankfurt, Germany and Cambridge,
195 UK), and Sec13 and NABP2 plasmids were obtained from Dr. Pagano (New York, USA). Pf1
196 immunoprecipitation samples were reduced, alkylated, and run into a gel to remove any
197 detergents and other mass spectrometry incompatible reagents. The gel plugs were
198 excised, digested with trypsin in-gel, extracted, and desalted (22). Following desalting the
199 peptide mixtures were gradient eluted directly into a Thermo Scientific Q Exactive mass
200 spectrometer. Data was searched using Sequest within the Proteome Discoverer software
201 suite for peptide and protein identifications.
202

203

204 **Results**

205 **Pf1 is required for proper mid-to-late gestation development**

206 To investigate the biological functions of Pf1 in a physiologically relevant system, we
207 generated a mouse strain harboring a genetic inactivation of the *Pf1* locus. Specifically, we
208 identified a mouse ES cell clone harboring a retroviral insertion in the 5' region of *Pf1*,
209 which results in the disruption of a splice acceptor site (Fig. 1A). We then used this ES cell
210 clone to derive a Pf1$^{+/-}$ mouse strain. Germline transmission of the mutant *Pf1* allele was
211 verified by PCR, and heterozygous mice were intercrossed to obtain Pf1$^{-/-}$ embryos (Fig.
212 1B). Genetic inactivation of *Pf1* in the Pf1$^{-/-}$ embryos was verified by qRT-PCR (Fig. 1C) and
213 embryonic development was followed. While *Pf1* heterozygous mice develop normally, no
214 live Pf1$^{-/-}$ mouse was born. Temporal analysis of embryonic development revealed that Pf1^{-}
215 $^{/-}$ embryos die at mid-to-late gestation, with diverse developmental defects, including
216 edema and internal hemorrhage (Fig. 1D and 1E). Moreover, macroscopic analysis of the
217 Pf1$^{-/-}$ embryos indicated a global growth retardation, where E14.5 Pf1$^{-/-}$ embryos were
218 comparable in size to E11.5 wild-type embryos (Fig. 1F and data not shown). Pf1$^{-/-}$
219 embryos also present impaired development of the skeleton, of the associated skeletal
220 muscle, and of the brain (Fig. 1F). To determine if the global growth retardation observed
221 at stage E14.5 results from a decrease in cell proliferation or, alternatively, from an
222 increase in cell apoptosis, we performed immunohistological staining on the whole embryo
223 at stage E14.5 for Ki67, a cell proliferation marker and Casp3, an effector caspase and a
224 marker of the cell commitment to apoptosis. No difference in the levels of Ki67 was
225 observed at this stage (Fig. 1G). In contrast, a localized increase in Casp3 were observed in
226 the liver of Pf1$^{-/-}$ embryos (Fig. 1H). Overall, these observations indicate that Pf1 is
227 essential for normal embryonic development, and Pf1 protects from aberrant apoptosis in a
228 tissue-specific manner.

229 **Pf1 prevents premature entry into replicative senescence**

230 We next generated Mouse Embryonic Fibroblasts (MEFs) from Pf1$^{+/+}$, Pf1$^{+/-}$ and Pf1$^{-/-}$
231 E14.5 embryos to assess the cellular function of Pf1. Following a standard 3T3 protocol, we

232 observed no significant differences in the ability of Pf1$^{+/+}$ and Pf1$^{+/-}$ MEFs to proliferate
233 (Fig. 2A). In contrast, Pf1$^{-/-}$ MEFs lost proliferative capacity as early as during the first cell
234 passaging. This result suggests that Pf1 functions to maintain a cellular proliferative state
235 in culture conditions. The decreased proliferative potential of Pf1$^{-/-}$ MEFs was associated
236 with a significant decrease in BrdU incorporation and an increase in SA-β-gal activity, a
237 marker of cellular senescence (Fig. 2B and 2C, respectively). Cellular senescence can be
238 triggered by the accumulation of irreparable DNA damage (23). Thus, we assessed the
239 levels of phosphorylated H2AX (γ-H2AX), a marker associated with DNA double-strand
240 breaks, in Pf1$^{-/-}$ and Pf1$^{+/+}$ MEFs. Consistent with the increased senescence detected in Pf1
241 null cells, Pf1$^{-/-}$ cells exhibited a strong activation of the DNA damage response, as
242 visualized by an increase in γ-H2AX signal compared to control cells (Fig. 2D). Thus, our
243 results suggest that Pf1 is essential to prevent premature cell cycle exit and entry into
244 cellular senescence.

245 **Pf1 is involved in maintaining the equilibrium of the rRNA processing pathway**

246 To identify the molecular mechanisms underlying the defects elicited by genetic
247 inactivation of *Pf1*, we next examined the impact of *Pf1* inactivation on the MEF
248 transcriptome. RNA extracted from wild-type and Pf1-null MEFs was profiled by
249 hybridization to a whole genome microarray. As shown in Figure 3A, Pf1 depletion led to
250 specific changes in gene expression, with 149 genes up-regulated and 323 genes down-
251 regulated by a 2-fold change ($p<0.05$) in Pf1$^{-/-}$ MEFs. Gene Ontology (GO) analysis using
252 the Database for Annotation, Visualization and Integrated Discovery (DAVID) analysis of
253 the transcripts differentially expressed in wild-type and Pf1 deficient cells revealed the
254 impact of Pf1 in multiple regulatory arms of the RNA biogenesis and maturation pathways
255 (Fig. 3B). Specifically, genetic inactivation of Pf1 resulted in a strong and significant
256 increase in the abundance of a large number of transcripts involved in ribosome biogenesis
257 and rRNA processing (Fig 3B and 3C). This finding was further validated by qRT-PCR for a
258 subset of genes including: Dimt1 (Dimethyladenosine Transferase 1 Homolog, an rRNA
259 methyltransferase); Pes1 (Pescadillo Ribosomal Biogenesis Factor 1, a component of
260 PeBoW complex, with roles in pre-rRNA processing and 60S ribosomal subunit

261 maturation); or Pa2G4 (Proliferation-Associated 2G4; involved in ribosome assembly and
262 the regulation of intermediate and late steps of rRNA processing) (Fig. 3D). Thus, our
263 results suggest that Pf1 plays an important role in regulating the levels of transcripts
264 involved in ribosomal biosynthesis and rRNA processing.

265 **Pf1$^{-/-}$ MEFs undergo changes in nucleolar structure**

266 The nucleolus is the site of ribosomal RNA synthesis and nascent ribosome assembly (24).
267 Previous studies pointed to a link between the nucleolar stress and cellular senescence (25,
268 26), although the molecular bases for this link remain elusive. To confirm our observations
269 that Pf1 deletion affects expression of the rRNA processing machinery, we analyzed by
270 immunofluorescence the levels of fibrillarin, SENP3 and UBF, three integral components of
271 the nucleolus that participate in rRNA processing. Fibrillarin is a rRNA 2'-O-
272 methyltransferase involved in the early stages of rRNA processing (27-30). SENP3 is a
273 SUMO-isopeptidase involved in the conversion of the 32S rRNA intermediate to the mature
274 28S rRNA in mammals (31-33). SENP3 also tightly associates with the nucleophosmin
275 NPM1, another central factor in ribosome biogenesis (34, 35). Fibrillarin and SENP3 exert
276 their function and are present in the outer two layers of the nucleoli: dense fibrillar
277 component and granular component. UBF is essential for the RNA Pol I pre-initiation
278 complex binding to enhancer regions of rDNA sequences; it exerts its functions in the
279 fibrillar center of the nucleolus, and also contributes to rRNA processing (27). As shown in
280 Figure 4, genetic inactivation Pf1 alters the shape and size of the nucleolus. Indeed, the
281 nucleolus of the Pf1 wild-type MEFs visualized by fibrillarin and SENP3
282 immunofluorescence appears as multiple small units (Fig. 4A, B). The staining pattern for
283 these markers was strikingly different in Pf1$^{-/-}$ MEFs, with an increase in fluorescence
284 intensity and a denser distribution in fewer spots within the nucleus, indicating a
285 reorganization of the nucleolus in these cells. However, disruption of the nucleolar
286 structure was not generalized since no difference was observed for intensity or
287 distribution of the UBF signal between Pf1$^{+/+}$ and Pf1$^{-/-}$ MEFs (Fig. 4C). This results suggest
288 that Pf1 controls the expression of specific components of rRNA processing machinery, and
289 affects the outer nucleolar structure.

290 **Proteomic characterization of Pf1-interacting factors identifies interactions with proteins**
291 **involved in ribosomal biogenesis**

292 To identify the molecular basis underlying the impact of Pf1 on nucleolar structure and
293 function, we aimed to identify novel Pf1- interacting proteins. To do so, we generated Flag-
294 tagged constructs of the wild-type Pf1, and two point-mutant Pf1 variants unable to
295 interact either with MRG15 or with histone H3 (mutants $Pf1^{F210A}$ and $Pf1^{D57N}$, respectively
296 (5, 36)). We then stably expressed the three constructs in the HeLa S3 cells, extracted
297 nuclear proteins, immunoprecipitated protein complexes containing the Pf1 construct
298 using anti-Flag beads, and analyzed the protein composition of the precipitated complexes
299 by LC-MS/MS. Silver-stained electrophoresis gels of the precipitated proteins revealed a
300 discrete band around 130 kDa, which corresponds to the apparent molecular weight of Pf1,
301 that was present in Pf1, $Pf1^{F210A}$ and $Pf1^{D57N}$ samples, but absent in the control HeLa cell
302 lysate infected with the pBabe empty vector (Fig. 5A). Moreover, a second prominent band
303 around 38 kDa, which corresponds to the apparent molecular weight of MRG15, was
304 observed only for Pf1 wild-type and $Pf1^{D57N}$, but not $Pf1^{F210A}$, as expected (Fig. 5A). The
305 precipitated proteins were then analyzed by nano-liquid chromatography tandem mass
306 spectrometry (LC-MS/MS) to identify the Pf1-associated proteins. As shown in Table 1, this
307 analysis identified most of the proteins previously known to be components of the
308 mammalian homolog of the Rpd3S complex, and to a lesser extent of the canonical Sin3-
309 HDAC complex. Notably, the enrichment confirmed the interaction between Pf1 and the
310 histone H3K4-specific demethylase KDM5A, EMSY, GATAD1, Sin3B, HDAC1, and MRG15 (5,
311 6). Thus, this result further confirmed a physical basis for the functional involvement of Pf1
312 in transcriptional regulation, and the stable association between Pf1, Sin3B, and a discrete
313 group of proteins previously known to be the components of the mammalian homolog of
314 the Rpd3S complex (3, 6, 37, 38).

315 Our analysis also points to the requirement of Pf1 association with MRG15 for Pf1
316 interaction with some proteins, including components of the canonical Sin3-HDAC
317 complex. Indeed, Table 2 lists the proteins that we identified as Pf1 interactors dependent
318 upon the Pf1 association with either MRG15 or histone H3 (proteins co-

319 immunoprecipitated with the wt Pf1 construct but not with the mutant Pf1^{F210A} or Pf1^{D57N}
320 constructs, respectively). Consistent with its known function in transcriptional regulation,
321 the proteins most abundantly co-immunoprecipitated with wt Pf1 are involved in
322 chromosome and chromatin organization, protein complex biogenesis, transcription, cell
323 cycle control and nuclear transport (Table 3). Importantly, LC-MS/MS analysis also
324 revealed the association of Pf1 with several proteins previously not identified as
325 interacting with Pf1. Table 4 lists some of these newly found possible Pf1 interactors,
326 grouped according to the Biological Process annotations. Interestingly, the LC-MS/MS
327 analysis of Pf1 associated complexes highlights proteins with roles in ribosome biogenesis,
328 similar to gene ontology terms associated with transcripts expressed at levels higher in Pf1
329 knockout than wt MEFs (Figure 3B). These proteins identified by LC-MS/MS include
330 ribosomal biogenesis protein LAS1L (LAS1L); nucleolar proteins 56 and 58 (NOP56,
331 NOP58); proline-, glutamic acid-, and leucine-rich protein 1 (PELP1); nucleophosmin 1
332 (NPM1); fibrillarin (FBL); testis expressed 10 (TEX10), WD repeat domain 3 and 18
333 (WDR3 and WDR18), BMS1 homolog, ribosome assembly protein (BMS1), as well as
334 ribosomal proteins S6, S7, S14, S 16 (RPS6, RPS6, RPS6, RPS6) and other (Table 4). A
335 complex comprising of PELP1, TEX10, WDR18, and SENP3 has been already described
336 (32). Additionally, the same report demonstrated that PELP1 and LAS1L are SUMOylated
337 by the SENP3 isopeptidase (32). SENP3 is a marker of the outer two layers of the nucleoli
338 (the dense fibrillar and granular components), and we have shown that anti SENP3
339 antibody staining of the nucleoli in Pf1-/- MEFs is more intense than in control cells,
340 marking a few large and clearly visible intranuclear structures, as opposed to more diffuse,
341 multiple small puncta in the wt cells. (see above and Fig. 4B). Finally, other examples of
342 newly identified Pf1 associated functional protein clusters include components of the
343 Anaphase Promoting Complex or proteins involved in transport through the nuclear
344 envelope (Table 4).

345 We thus conducted co-immunoprecipitation (coIP) experiments using tagged constructs of
346 Pf1 and selected potential novel Pf1 interaction candidates identified in our LC-MS/MS
347 experiment, as well as an additional component of the Anaphase Promoting Complex,
348 namely ACP8. Compared to our negative control SOSS complex subunit B1 (NABP2, Fig.

349 5E), all the coIPs performed showed a clear interaction between Pf1 and the proteins
350 tested (Fig. 5B-D). The interaction with Pf1 was particularly strong for PELP1 (Fig. 5B) and
351 Sec13 (Fig. 5D). Altogether, these results corroborate the findings of our LC-MS/MS
352 analysis and suggest that Pf1 directly contributes to the maintenance of nucleolar functions
353 through its interaction with proteins that participate to ribosomal biogenesis. Along with
354 the demonstration that Pf1 regulates the transcription of genes involved in the rRNA
355 pathway, our results indicate that Pf1 may coordinate transcriptional and post-
356 transcriptional steps of ribosomal biogenesis.

357

358 **Discussion**

359 We undertook the generation and characterization of the Pf1 knockout mice in order to
360 define the physiological role of Pf1. Pf1 was first identified as a component of the Sin3-
361 HDAC complex. Specifically, Pf1 appears to interact directly with the Sin3 scaffold proteins,
362 Sin3A or Sin3B, depending on the experimental and/or cellular context. Biochemical
363 studies have now revealed that Pf1 serves as an integral component of a small HDAC1/2
364 containing complex that comprises the Sin3B, HDAC1/2 and Mrg15 proteins (2-5). Pf1, like
365 Sin3B, Mrg15 or HDAC1/2, is essential for embryonic development. However, the cellular
366 phenotypes elicited upon Pf1 inactivation that we report here differ drastically from those
367 resulting from genetic deletion of Sin3B. Indeed, we have previously demonstrated that
368 Sin3B inactivation in primary mouse embryonic fibroblasts does not impact cellular
369 proliferation in normal culture conditions, but impairs cell cycle exit triggered by pro-
370 quiescence or pro-senescence signals (10-12). By contrast, Pf1 null MEFs are unable to
371 sustain proliferation, and they enter spontaneous premature senescence in normal culture
372 conditions. The discrepancy between Pf1 and Sin3B-null MEFs phenotypes may be
373 attributed to the partial redundancy between Sin3B and its close paralog Sin3A. Indeed,
374 Sin3A inactivation is incompatible with cellular proliferation. While our previous report
375 suggested that the interaction between Sin3B and Pf1 is tighter than the one between
376 Sin3A and Pf1 (6), it is important to note that our proteomic study clearly identified Sin3A
377 as a Pf1 interactor. Interestingly, the phenotypes elicited upon Mrg15 inactivation are
378 reminiscent of those uncovered in Pf1 null cells. Indeed, Tominaga and colleagues observed
379 that *Mrg15*-/- embryos present growth retardation and delayed development of many
380 organs and tissues, as well as defective cell proliferation and differentiation (17).
381 Interestingly, Mrg15-null cells adopt senescent phenotypes prematurely and cease to
382 proliferate earlier than their wild-type counterparts, a phenotype that is shared by Pf1 null
383 MEFs. While Mrg15 is an integral part of two distinct chromatin modifying complexes, the
384 Sin3-Pf1-HDAC complex and the NuA4 complex, the phenotypes elicited upon Mrg15
385 inactivation are strikingly similar to those we report here in Pf1 null embryos and cells.
386 Thus, it is tempting to speculate that the resembling phenotypes elicited upon Mrg15 or Pf1
387 inactivation reflect the functional interaction between the two proteins. In that aspect, it is

388 important to note that Eaf3, the yeast homolog of Mrg15, is dispensable for a functional
389 NuA4 complex (39).
390 Cellular senescence is a stable cell-cycle arrest in response to various cellular stresses (40-
391 42). Many stimuli trigger senescence in primary cells. This includes oxidative stress, DNA
392 damage, the expression of activated oncogenes (oncogene-induced senescence), or serial
393 passaging, which drives to replicative senescence (43). Thus, senescence is often seen as a
394 mechanism to prevent damaged or mutated cells from proliferating uncontrollably (44).
395 Interestingly, senescent cells often present morphological changes in the nucleolus, with a
396 single, very prominent nucleolus instead of a few smaller ones (25, 26). Our results
397 indicate Pf1 controls specific steps of the ribosome biogenesis, such as splicing, covalent
398 modifications, and maturation of the pre-ribosomal RNA transcripts, and that the changes
399 observed in the nucleoli of Pf1 -/- MEFs are unlikely to be an unspecific, secondary
400 consequence of the changes in the rate at which the Pf1 -/- cells proliferate. Interestingly, it
401 was reported earlier that premature aging in yeast mutants for the Werner helicase Sgs1
402 correlates with alterations of the nucleolar structure, reminiscent of what we observe in
403 Pf1 -/- MEFs (45). Given the functional link between senescence and aging in mammals
404 (46) it is tempting to speculate that Pf1 engages a program that coordinates nucleolar
405 integrity and prevention of premature aging. In that aspect, it is intriguing to note the
406 recent demonstration that perturbation of ribosomal biogenesis results in the activation of
407 a senescence program in mammalian cells (47).
408 It is also worth mentioning that the yeast Rpd3-Sin3 complex has been shown to catalyse
409 histone H4 deacetylation at rDNA chromatin, through this mechanism- to control RNA
410 polymerase I localization to and rDNA transcription, and in consequence the shape and size
411 of the nucleolus in yeast cells (48). Experiments in mammalian cells suggest that NoRC, a
412 SNF2h-containing NucleOlar chromatin Remodelling Complex, silences the rDNA locus by
413 targeting the Sin3 corepressor complex to rDNA promoters (49). Given our observation
414 that only the outer layers of the nucleolus are altered in Pf1 -/- MEFs, it is unlikely that Pf1
415 alters ribosomal biogenesis directly through the modulation of rDNA transcription. Indeed,
416 we were unable to detect alteration in the amount of transcripts corresponding to rRNA in
417 the absence of Pf1 (data not shown). Together, these observations point to a role of Pf1 in
418 post-transcriptional events linked to ribosomal biogenesis.

419 Our co-immunoprecipitation experiments confirmed the interaction of Pf1 with PELP1,
420 LAS1L, and NPM1. Previous studies showed that inactivation of these proteins can, directly
421 or not, induce senescence, similar to what we observed during Pf1 inactivation. First, NPM1
422 was recently identified to control a p53-mediated cellular senescence. Using a model of
423 colorectal cancer, Wong and colleagues showed that the suppression of NPM1 activity
424 reduces viability, and enhances senescence and cell cycle arrest (50). Second, PELP1
425 silencing was also shown to promote senescence and inhibit the proliferation, colony
426 formation, migration, invasion and xenograft in the same colorectal cancer model (51).
427 Finally, LAS1L inactivation has been showed to result in a G1 arrest, linking LAS1L to cell
428 cycle progression (52). Moreover, SENP3, which we showed is more abundant in the Pf1 -/-
429 MEFS than in the control cells, interacts with NPM1 (31, 32, 35) and forms a nucleolar
430 complex with PELP1 and LAS1L (52). If our experiments cannot completely rule out an
431 indirect role of Pf1 in ribosomal biogenesis, the results of our LS-MS/MS and subsequent
432 co-IPs analyses suggest that the effect of Pf1 on nucleolar functions might not be mediated,
433 or at least mediated not solely by the Pf1 association with the Sin3-MRG15-HDAC complex.
434 It will be therefore particularly important to perform an exhaustive characterization of the
435 different protein complexes for which Pf1 is present, in order to understand how Pf1
436 executes its function in ribosome biogenesis and to discriminate between this function in
437 ribosome biogenesis to the one that has already been characterized as a transcriptional
438 regulator. Indeed, we have previously shown that the Pf1 complex modulates RNAPII-
439 driven transcription. In that aspect, it is important to note that recent findings have
440 demonstrated that specific factors can coordinate the transcriptional regulation of
441 ribosomal proteins and the ribosomal RNA maturation (53). Our results suggest that Pf1
442 and its associated chromatin modifying activities may also coordinate several steps in the
443 generation of functional ribosomal subunits.
444 In conclusion, our study point to a central function for a chromatin associated protein in
445 the regulation of ribosomal biogenesis, and senescence. Whether this property of Pf1
446 contributes to alteration of nucleolar functions and accumulation of senescent cells in
447 physiological settings such as replicative aging or response to exogenous stress remains to
448 be investigated.
449

Acknowledgements

The authors would like to thank the staff of NYU Langone School of Medicine Dr. Ueberheide and the Proteomics Resource Center, and Dr. Heguy and the Genome Technology Center for assistance (both supported in part by an NIH/NCI support grant P30CA016087) with the proteomics and the microarray experiments respectively, and Dr. Esthelle Hoedt for help with proteomics data analyses. We also thank Dr. Beatriz Fontoura, Dr. John Goodier, Dr. Daisuke Izawa, Dr. Stefan Muller and Dr. Celine Verheggen for the generous gift of reagents. Work reported here was supported by the National Institute of Health (R01CA148639 and R21CA155736 to GD), the Samuel Waxman Cancer Research Foundation (GD) and a Feinberg NYU individual grant (GD). KM was supported by the Departmental Training Grant 5-T32CA9161-40. The Mass Spectrometric experiments were in part supported by the Cancer Center Support Grant, P30CA016087, at the Laura and Isaac Perlmutter Cancer Center.

464 References:

465 1. **Musselman CA, Kutateladze TG.** 2011. Handpicking epigenetic marks with PHD fingers.
466 Nucleic Acids Res **39:**9061-9071.
467 2. **Yochum GS, Ayer DE.** 2001. Pf1, a novel PHD zinc finger protein that links the TLE
468 corepressor to the mSin3A-histone deacetylase complex. Mol Cell Biol **21:**4110-4118.
469 3. **Hayakawa T, Ohtani Y, Hayakawa N, Shinmyozu K, Saito M, Ishikawa F, Nakayama J.**
470 2007. RBP2 is an MRG15 complex component and down-regulates intragenic histone H3
471 lysine 4 methylation. Genes Cells **12:**811-826.
472 4. **Yochum GS, Ayer DE.** 2002. Role for the mortality factors MORF4, MRGX, and MRG15 in
473 transcriptional repression via associations with Pf1, mSin3A, and Transducin-Like
474 Enhancer of Split. Mol Cell Biol **22:**7868-7876.
475 5. **Xie T, Graveline R, Kumar GS, Zhang Y, Krishnan A, David G, Radhakrishnan I.** 2012.
476 Structural basis for molecular interactions involving MRG domains: implications in
477 chromatin biology. Structure **20:**151-160.
478 6. **Jelinic P, Pellegrino J, David G.** 2011. A novel mammalian complex containing Sin3B
479 mitigates histone acetylation and RNA polymerase II progression within transcribed loci.
480 Mol Cell Biol **31:**54-62.
481 7. **Kaadige MR, Ayer DE.** 2006. The polybasic region that follows the plant homeodomain
482 zinc finger 1 of Pf1 is necessary and sufficient for specific phosphoinositide binding. J
483 Biol Chem **281:**28831-28836.
484 8. **Strobl-Mazzulla PH, Bronner ME.** 2012. A PHD12-Snail2 repressive complex
485 epigenetically mediates neural crest epithelial-to-mesenchymal transition. J Cell Biol
486 **198:**999-1010.
487 9. **Bansal N, Petrie K, Christova R, Chung CY, Leibovitch BA, Howell L, Gil V, Sbirkov Y, Lee**
488 **E, Wexler J, Ariztia EV, Sharma R, Zhu J, Bernstein E, Zhou MM, Zelent A, Farias E,**
489 **Waxman S.** 2015. Targeting the SIN3A-PF1 interaction inhibits epithelial to
490 mesenchymal transition and maintenance of a stem cell phenotype in triple negative
491 breast cancer. Oncotarget **6:**34087-34105.
492 10. **David G, Grandinetti KB, Finnerty PM, Simpson N, Chu GC, Depinho RA.** 2008. Specific
493 requirement of the chromatin modifier mSin3B in cell cycle exit and cellular
494 differentiation. Proc Natl Acad Sci U S A **105:**4168-4172.
495 11. **Grandinetti KB, David G.** 2008. Sin3B: an essential regulator of chromatin modifications
496 at E2F target promoters during cell cycle withdrawal. Cell Cycle **7:**1550-1554.
497 12. **Grandinetti KB, Jelinic P, DiMauro T, Pellegrino J, Fernandez Rodriguez R, Finnerty PM,**
498 **Ruoff R, Bardeesy N, Logan SK, David G.** 2009. Sin3B expression is required for cellular
499 senescence and is up-regulated upon oncogenic stress. Cancer Res **69:**6430-6437.
500 13. **Rielland M, Cantor DJ, Graveline R, Hajdu C, Mara L, Diaz Bde D, Miller G, David G.**
501 2014. Senescence-associated SIN3B promotes inflammation and pancreatic cancer
502 progression. J Clin Invest **124:**2125-2135.
503 14. **Lagger G, O'Carroll D, Rembold M, Khier H, Tischler J, Weitzer G, Schuettengruber B,**
504 **Hauser C, Brunmeir R, Jenuwein T, Seiser C.** 2002. Essential function of histone
505 deacetylase 1 in proliferation control and CDK inhibitor repression. EMBO J **21:**2672-
506 2681.

15. **Montgomery RL, Davis CA, Potthoff MJ, Haberland M, Fielitz J, Qi X, Hill JA, Richardson JA, Olson EN.** 2007. Histone deacetylases 1 and 2 redundantly regulate cardiac morphogenesis, growth, and contractility. Genes Dev **21:**1790-1802.
16. **Wilting RH, Yanover E, Heideman MR, Jacobs H, Horner J, van der Torre J, DePinho RA, Dannenberg JH.** 2010. Overlapping functions of Hdac1 and Hdac2 in cell cycle regulation and haematopoiesis. EMBO J **29:**2586-2597.
17. **Tominaga K, Kirtane B, Jackson JG, Ikeno Y, Ikeda T, Hawks C, Smith JR, Matzuk MM, Pereira-Smith OM.** 2005. MRG15 regulates embryonic development and cell proliferation. Mol Cell Biol **25:**2924-2937.
18. **Serrano M, Lin AW, McCurrach ME, Beach D, Lowe SW.** 1997. Oncogenic ras provokes premature cell senescence associated with accumulation of p53 and p16INK4a. Cell **88:**593-602.
19. **Reich M, Liefeld T, Gould J, Lerner J, Tamayo P, Mesirov JP.** 2006. GenePattern 2.0. Nat Genet **38:**500-501.
20. **Huang da W, Sherman BT, Lempicki RA.** 2009. Systematic and integrative analysis of large gene lists using DAVID bioinformatics resources. Nat Protoc **4:**44-57.
21. **Huang da W, Sherman BT, Zheng X, Yang J, Imamichi T, Stephens R, Lempicki RA.** 2009. Extracting biological meaning from large gene lists with DAVID. Curr Protoc Bioinformatics **Chapter 13:**Unit 13 11.
22. **Cotto-Rios XM, Bekes M, Chapman J, Ueberheide B, Huang TT.** 2012. Deubiquitinases as a signaling target of oxidative stress. Cell Rep **2:**1475-1484.
23. **Di Micco R, Sulli G, Dobreva M, Liontos M, Botrugno OA, Gargiulo G, dal Zuffo R, Matti V, d'Ario G, Montani E, Mercurio C, Hahn WC, Gorgoulis V, Minucci S, d'Adda di Fagagna F.** 2011. Interplay between oncogene-induced DNA damage response and heterochromatin in senescence and cancer. Nat Cell Biol **13:**292-302.
24. **Boisvert FM, van Koningsbruggen S, Navascues J, Lamond AI.** 2007. The multifunctional nucleolus. Nat Rev Mol Cell Biol **8:**574-585.
25. **Holmberg Olausson K, Nister M, Lindstrom MS.** 2012. p53 -Dependent and -Independent Nucleolar Stress Responses. Cells **1:**774-798.
26. **Kar B, Liu B, Zhou Z, Lam YW.** 2011. Quantitative nucleolar proteomics reveals nuclear re-organization during stress- induced senescence in mouse fibroblast. BMC Cell Biol **12:**33.
27. **Sobol M, Yildirim S, Philimonenko VV, Marasek P, Castano E, Hozak P.** 2013. UBF complexes with phosphatidylinositol 4,5-bisphosphate in nucleolar organizer regions regardless of ongoing RNA polymerase I activity. Nucleus **4:**478-486.
28. **Newton K, Petfalski E, Tollervey D, Caceres JF.** 2003. Fibrillarin is essential for early development and required for accumulation of an intron-encoded small nucleolar RNA in the mouse. Mol Cell Biol **23:**8519-8527.
29. **Adams PD.** 2007. Remodeling of chromatin structure in senescent cells and its potential impact on tumor suppression and aging. Gene **397:**84-93.
30. **Tollervey D, Lehtonen H, Jansen R, Kern H, Hurt EC.** 1993. Temperature-sensitive mutations demonstrate roles for yeast fibrillarin in pre-rRNA processing, pre-rRNA methylation, and ribosome assembly. Cell **72:**443-457.

550 31. **Finkbeiner E, Haindl M, Raman N, Muller S.** 2011. SUMO routes ribosome maturation.
551 Nucleus **2:**527-532.
552 32. **Finkbeiner E, Haindl M, Muller S.** 2011. The SUMO system controls nucleolar
553 partitioning of a novel mammalian ribosome biogenesis complex. EMBO J **30:**1067-1078.
554 33. **Grisendi S, Mecucci C, Falini B, Pandolfi PP.** 2006. Nucleophosmin and cancer. Nat Rev
555 Cancer **6:**493-505.
556 34. **Haindl M, Harasim T, Eick D, Muller S.** 2008. The nucleolar SUMO-specific protease
557 SENP3 reverses SUMO modification of nucleophosmin and is required for rRNA
558 processing. EMBO Rep **9:**273-279.
559 35. **Raman N, Nayak A, Muller S.** 2014. mTOR signaling regulates nucleolar targeting of the
560 SUMO-specific isopeptidase SENP3. Mol Cell Biol **34:**4474-4484.
561 36. **Kumar GS, Chang W, Xie T, Patel A, Zhang Y, Wang GG, David G, Radhakrishnan I.**
562 2012. Sequence requirements for combinatorial recognition of histone H3 by the
563 MRG15 and Pf1 subunits of the Rpd3S/Sin3S corepressor complex. J Mol Biol **422:**519-
564 531.
565 37. **Benevolenskaya EV, Murray HL, Branton P, Young RA, Kaelin WG, Jr.** 2005. Binding of
566 pRB to the PHD protein RBP2 promotes cellular differentiation. Mol Cell **18:**623-635.
567 38. **Florens L, Carozza MJ, Swanson SK, Fournier M, Coleman MK, Workman JL, Washburn**
568 **MP.** 2006. Analyzing chromatin remodeling complexes using shotgun proteomics and
569 normalized spectral abundance factors. Methods **40:**303-311.
570 39. **Mitchell L, Lambert JP, Gerdes M, Al-Madhoun AS, Skerjanc IS, Figeys D, Baetz K.** 2008.
571 Functional dissection of the NuA4 histone acetyltransferase reveals its role as a genetic
572 hub and that Eaf1 is essential for complex integrity. Mol Cell Biol **28:**2244-2256.
573 40. **Collado M.** 2010. Exploring a 'pro-senescence' approach for prostate cancer therapy by
574 targeting PTEN. Future Oncol **6:**687-689.
575 41. **Collado M, Serrano M.** 2010. Senescence in tumours: evidence from mice and humans.
576 Nat Rev Cancer **10:**51-57.
577 42. **Sharpless NE, Sherr CJ.** 2015. Forging a signature of in vivo senescence. Nat Rev Cancer
578 **15:**397-408.
579 43. **Dimauro T, David G.** 2009. Chromatin modifications: the driving force of senescence
580 and aging? Aging (Albany NY) **1:**182-190.
581 44. **Kuilman T, Michaloglou C, Mooi WJ, Peeper DS.** 2010. The essence of senescence.
582 Genes Dev **24:**2463-2479.
583 45. **Sinclair DA, Mills K, Guarente L.** 1997. Accelerated aging and nucleolar fragmentation in
584 yeast sgs1 mutants. Science **277:**1313-1316.
585 46. **van Deursen JM.** 2014. The role of senescent cells in ageing. Nature **509:**439-446.
586 47. **Nishimura K, Kumazawa T, Kuroda T, Katagiri N, Tsuchiya M, Goto N, Furumai R,**
587 **Murayama A, Yanagisawa J, Kimura K.** 2015. Perturbation of ribosome biogenesis
588 drives cells into senescence through 5S RNP-mediated p53 activation. Cell Rep **10:**1310-
589 1323.
590 48. **Tsang CK, Bertram PG, Ai W, Drenan R, Zheng XF.** 2003. Chromatin-mediated regulation
591 of nucleolar structure and RNA Pol I localization by TOR. EMBO J **22:**6045-6056.

592 49. **Zhou Y, Santoro R, Grummt I.** 2002. The chromatin remodeling complex NoRC targets
593 HDAC1 to the ribosomal gene promoter and represses RNA polymerase I transcription.
594 EMBO J **21:**4632-4640.
595 50. **Wong JC, Hasan MR, Rahman M, Yu AC, Chan SK, Schaeffer DF, Kennecke HF, Lim HJ,**
596 **Owen D, Tai IT.** 2013. Nucleophosmin 1, upregulated in adenomas and cancers of the
597 colon, inhibits p53-mediated cellular senescence. Int J Cancer **133:**1567-1577.
598 51. **Ning Z, Zhang Y, Chen H, Wu J, Song T, Wu Q, Liu F.** 2014. PELP1 suppression inhibits
599 colorectal cancer through c-Src downregulation. Oxid Med Cell Longev **2014:**193523.
600 52. **Castle CD, Cassimere EK, Denicourt C.** 2012. LAS1L interacts with the mammalian Rix1
601 complex to regulate ribosome biogenesis. Mol Biol Cell **23:**716-728.
602 53. **Calo E, Flynn RA, Martin L, Spitale RC, Chang HY, Wysocka J.** 2015. RNA helicase DDX21
603 coordinates transcription and ribosomal RNA processing. Nature **518:**249-253.
604

605

606 **Figure 1. Pf1 is required for proper mid-to-late gestation development** (A) Schematic
607 representation of the wild-type (top) or mutated (bottom) allele for *Pf1*. (B) Endpoint
608 genotyping PCR on 14.5 dpc embryos of the indicated genotype for *Pf1*. (C) Quantitative
609 Reverse-Transcriptase PCR (qRT-PCR) for the expression of *Pf1* in $Pf1^{+/+}$ and $Pf1^{-/-}$
610 embryos. (D) Genotype distribution of embryos from Pf1 heterozygotes intercrosses in a
611 C57BL/6 background (E, embryonic day). The number of animals analyzed per genotype
612 and time point are indicated as well as the corresponding percentage in parentheses. (E)
613 Representative picture of $Pf1^{+/+}$ and $Pf1^{-/-}$ embryos at E14.5. (F) Hematoxylin- and Eosin-
614 stained sections performed on the whole $Pf1^{+/+}$ (left) and $Pf1^{-/-}$ (right) embryos. (G)
615 Immunohistochemistry (IHC) staining for Ki67 on $Pf1^{+/+}$ (left) and $Pf1^{-/-}$ (right) embryos
616 on day 14.5 dpc. (H) IHC staining for Casp3 on $Pf1^{+/+}$ (left) and $Pf1^{-/-}$ (middle) embryos on
617 day 14.5 dpc. Right panel corresponds to a magnification of the fetal liver in $Pf1^{-/-}$ embryos.
618
619 **Figure 2. Pf1 prevents premature entry into replicative senescence**. (A) Growth curves using
620 a 3T3 protocol on early-passage $Pf1^{+/+}$, $Pf1^{+/-}$ and $Pf1^{-/-}$ embryos. (B) BrdU incorporation
621 after a 2-hour pulse of 20 μM by $Pf1^{+/+}$ and $Pf1^{-/-}$ early passage primary MEFs. For each
622 conditions, 200 cells were at least counted (n=3). (C) Quantification of SA-β-gal-positive
623 cells in $Pf1^{+/+}$ and $Pf1^{-/-}$ early passage primary MEFs. Left panel shows a representative
624 picture of SA-β-gal stain for both genotype. Right panel represents the percentage of SA-β-
625 gal-positive cells after counting at least 200 cells (n=3). (D) γH2A.X immunofluorescence
626 staining for $Pf1^{+/+}$ and $Pf1^{-/-}$ early passage primary MEFs. Left panel shows a
627 representative picture of γH2A.X positive cells in $Pf1^{+/+}$ and $Pf1^{-/-}$ MEFs. Right panel
628 represents the percentage of γH2A.X positive cells after counting at least 200 cells (n=3).
629
630 **Figure 3. Pf1 is involved in maintaining the equilibrium of the rRNA processing pathway** (A)
631 Venn diagram representation of the differential gene expression $Pf1^{+/+}$ and $Pf1^{-/-}$ early
632 passage primary MEFs. (B) Pathway enrichment analysis using DAVID gene ontology of
633 genes transcriptionally induced upon Pf1 deletion in MEFs. GO analyses were made on
634 genes that presented at least a 2-fold significant expression change in $Pf1^{-/-}$ early passage
635 primary MEFs compared to $Pf1^{+/+}$ early passage primary MEFs ($p<0.05$). Bars represent
636 fold enrichment of the pathway in order of significance (P values) listed on the right of the

637 bars. Functional categorizations of differentially expressed genes upon knock-out of *Pf1*
638 were analyzed by Gene Ontology Biological Process (GO_BP). (C) Heat map representation
639 of enriched expression for ribonucleoprotein complex biogenesis, ribosome biogenesis and
640 rRNA processing pathways in $Pf1^{+/+}$ and $Pf1^{-/-}$ MEFs. Heat map represents top enriched
641 genes in $Pf1^{-/-}$ MEFs compared to $Pf1^{+/+}$ MEFs. NES, normalized enrichment score (red,
642 high expression; blue low expression). (D) Quantitative RT-PCR for a subset of genes
643 present in the ribonucleoprotein complex biogenesis, ribosome biogenesis and rRNA
644 processing pathways. $Pf1^{-/-}$ mRNA expression levels are relative to the $Pf1^{+/+}$ expression
645 levels (n=3).

646

647 **Figure 4. Pf1 inactivation is associated to morphological changes in the nucleolus**.
648 Representative immunofluorescence staining on $Pf1^{+/+}$ and $Pf1^{-/-}$ MEFs for Fibrillarin (A),
649 SENP3 (B) and UBF (C).

650

651 **Figure 5. Pf1 interaction network**. (A) Pf1-associated proteins immunopurified from HELA
652 S3 nuclear extract (NE) stably expressing a flag-tagged version of wt Pf1 or two point
653 mutants versions ($Pf1^{F210A}$ and $Pf1^{D57N}$). Proteins were resolved by SDS-PAGE and revealed
654 by a silver staining (B-D) Co-Immunoprecipiation analysis to confirm the association of Pf1
655 with selected proteins: involved in ribosome biogenesis pathway (B), and components of
656 the anaphase promoting complex (C) and nucleopore complex (D); (E) negative control for
657 the co-immunoprecipitation experiments.

658

659 **Table 1. Composition of the main complex associated with Pf1**.

660

661 **Table 2. List of Proteins for which the substitution F210A or D57N affects the association**
662 **with Pf1.**

663

664 **Table 3. Gene Ontology analysis of proteins that associate with Pf1**. Entries were grouped
665 according to their association with indicated Gene Ontology Biological Process terms. fold
666 enrichment and P-values shown were obtained using the DAVID Functional Annotation

667 Tool and the list of proteins most abundantly associated with wt Pf1 in our LS-MS/MS
668 analysis.
669
670 **Table 4. Novel proteins found to associate with Pf1**. Selected proteins found to associate
671 with Pf1 through LS-MS/MS analysis. Genes are grouped according to their association with
672 indicated Gene Ontology Biological Process terms. P-values indicated were obtained using
673 the DAVID Functional Annotation Tool and the list of all proteins identified as associated
674 with wt Pf1 in our LS-MS/MS analysis

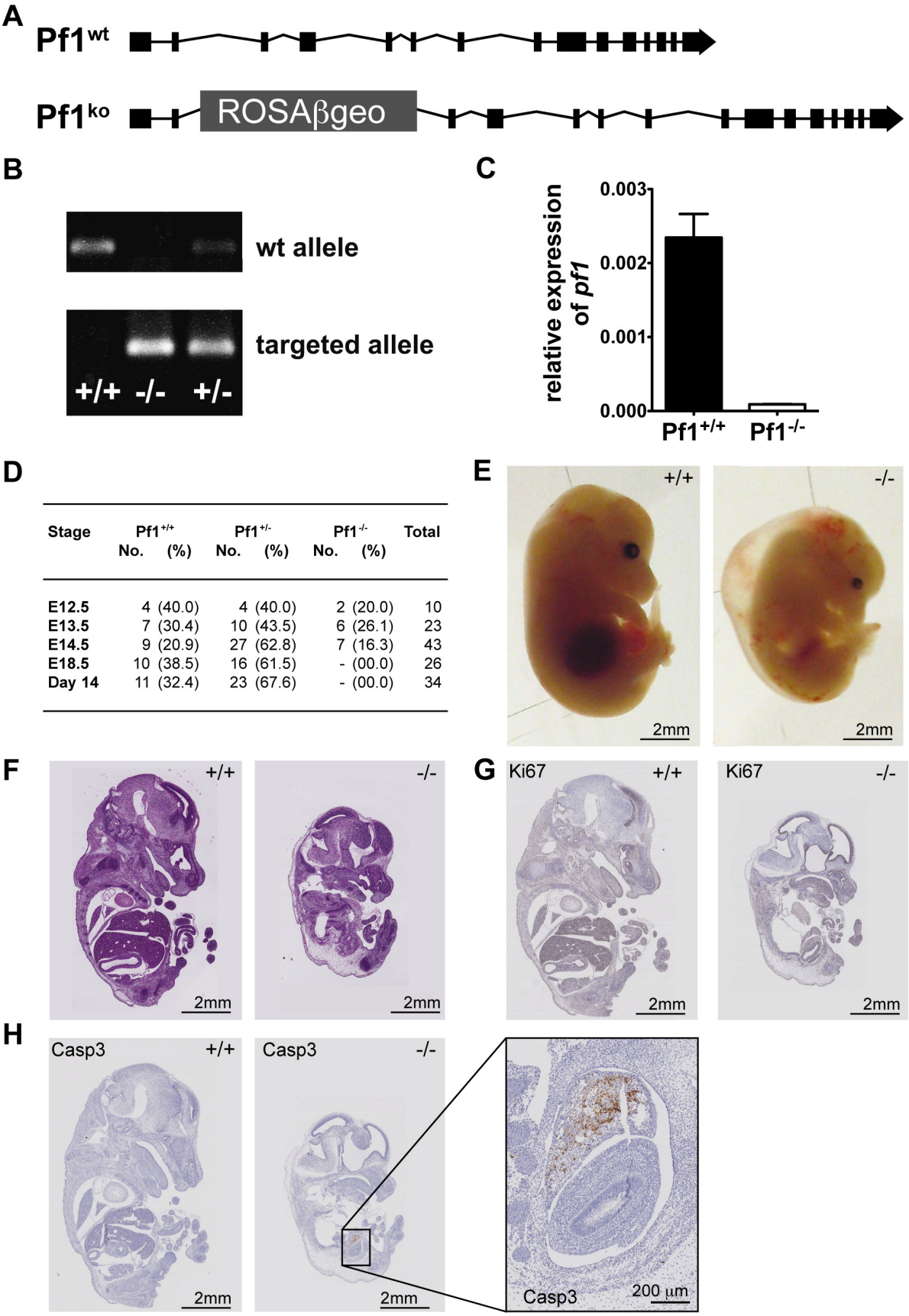

Stage	Pf1+/+ No.	Pf1+/+ (%)	Pf1+/- No.	Pf1+/- (%)	Pf1-/- No.	Pf1-/- (%)	Total
E12.5	4	(40.0)	4	(40.0)	2	(20.0)	10
E13.5	7	(30.4)	10	(43.5)	6	(26.1)	23
E14.5	9	(20.9)	27	(62.8)	7	(16.3)	43
E18.5	10	(38.5)	16	(61.5)	-	(00.0)	26
Day 14	11	(32.4)	23	(67.6)	-	(00.0)	34

A

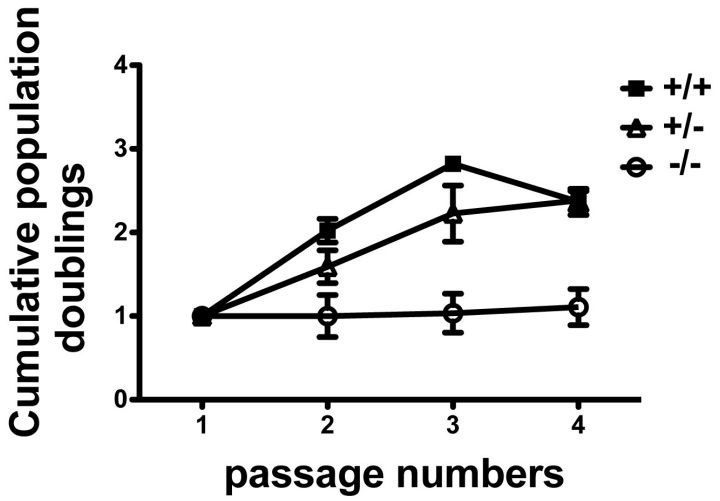

B

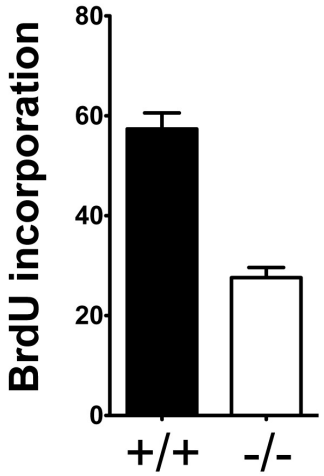

C

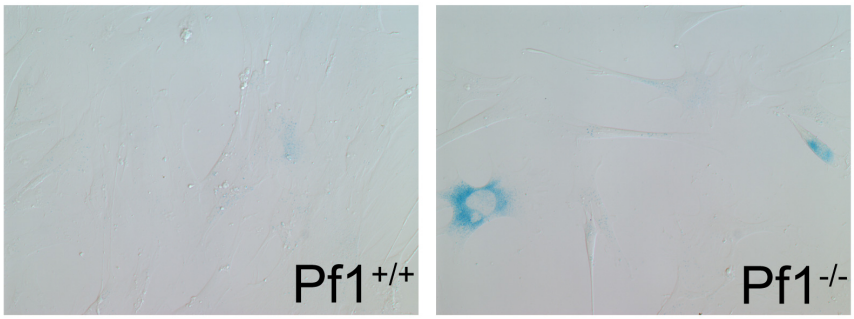

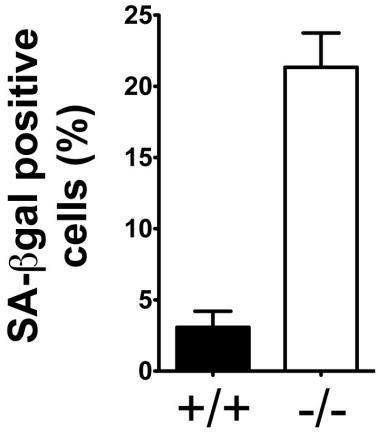

D

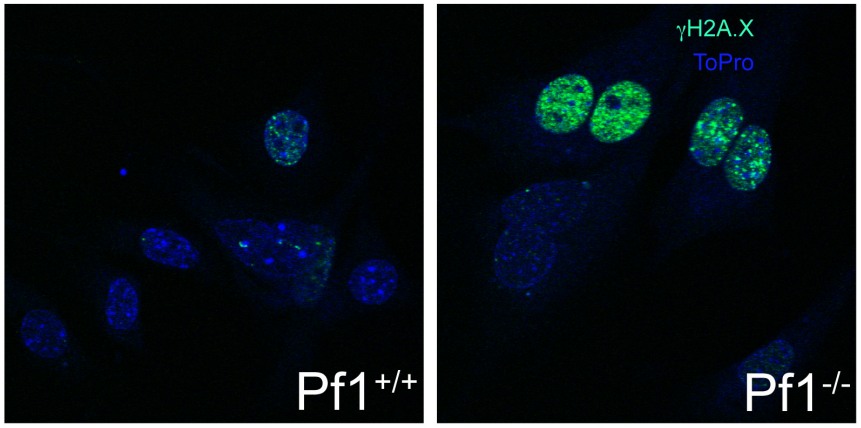

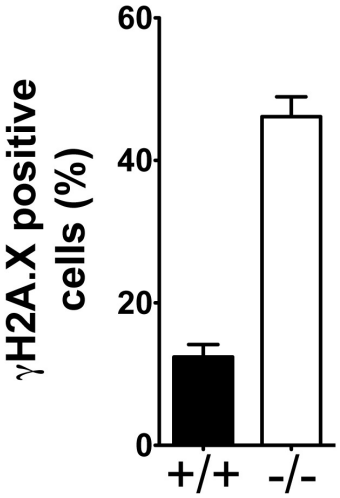

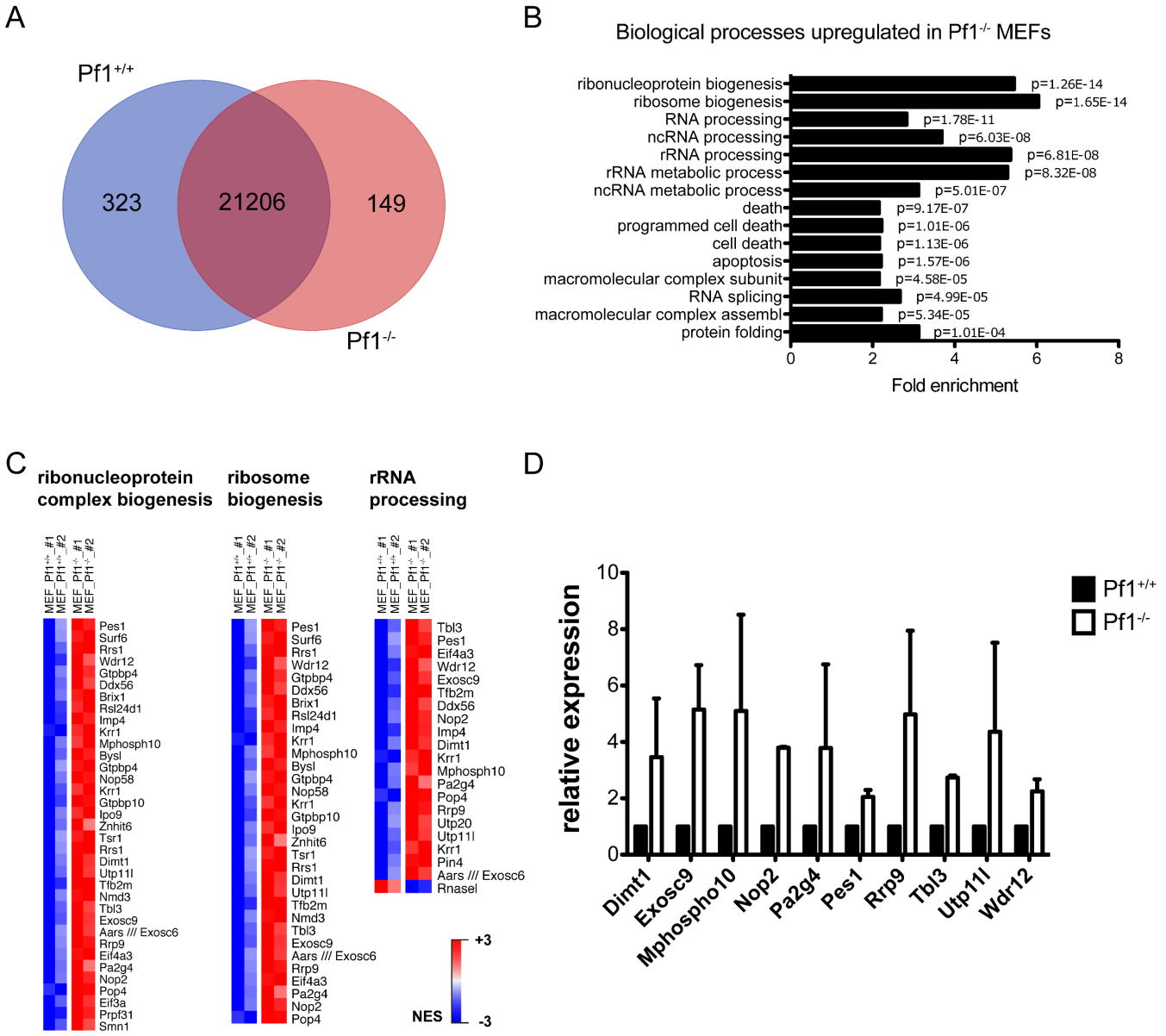

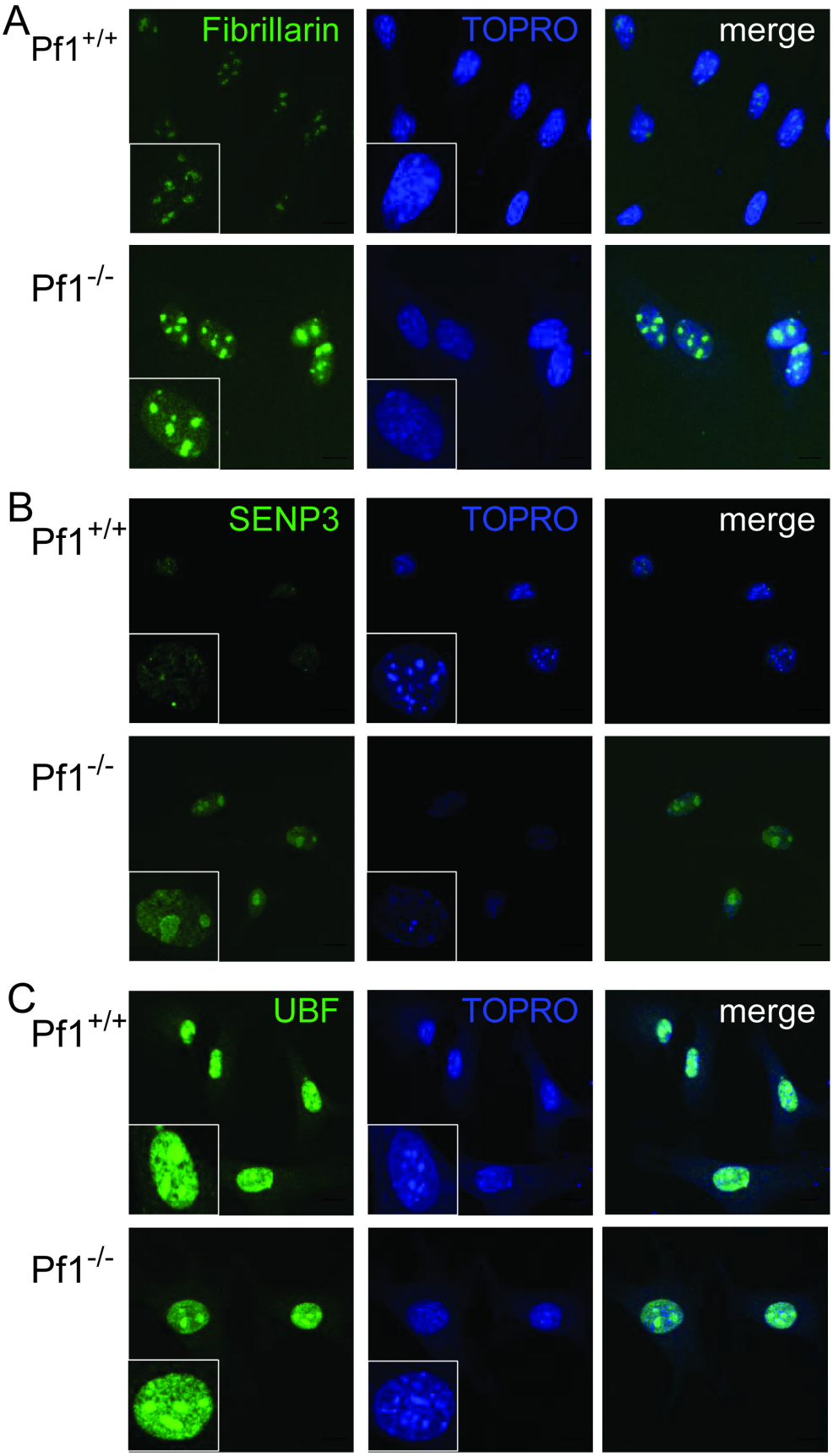

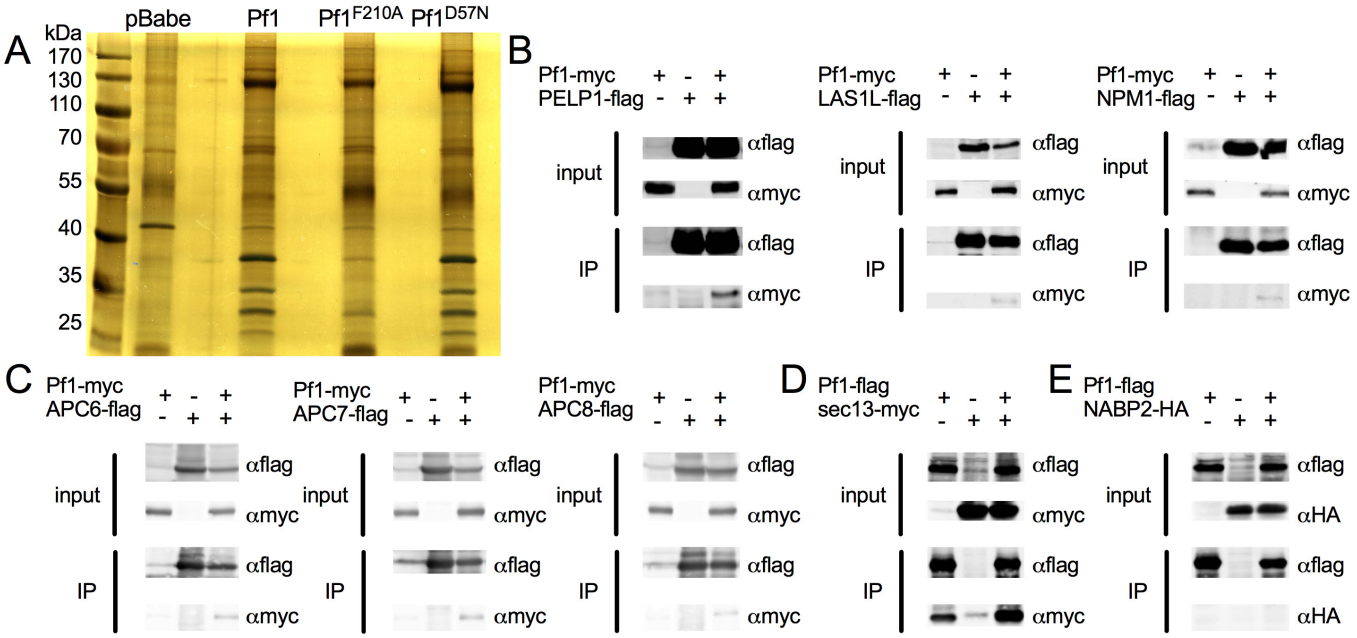

Description	Score	#peptides	MW (kDa)
Pf1-SIN3B core complex			
GATAD1	63.67	11	28.7
MORF4L2	121.93	18	32.3
KDM5A	329.82	61	192.0
SIN3B	261.28	38	129.3
EMSY	205.31	35	141.4
ZNF131	31.17	7	67.3
MORF4L1	223.52	23	37.2
SIN3A complex			
SIN3A	196.66	37	145.1
SDS3	45.29	77	38.1
SAP30	7.33	2	23.3
SAP130	24.36	7	113.9
HDAC1	114.20	12	55.1
Rbbp7	74.59	11	47.8
Rbbp4	27.46	5	46.1

Table 1.

Proteins specifically absent in $Pf1^{F210A}$, $Pf1^{D57N}$, or both IP samples	
$Pf1^{F210A}$	MORF4L2, APC1, APC7, POLR2B, RANGP1, ZBTB7A
$Pf1^{D57N}$	CDK9
$Pf1^{F210A}$ and $Pf1^{D57N}$	SIN3A, KPNB1, USP7, CCAR2

Table 2.

Biological Processes Term	Fold Enrichment	p-value
Chromosome organization	5.51	1.30E-07
Protein complex biogenesis	5.29	2.19E-07
Protein complex assembly	5.29	2.19E-07
Chromatin organization	6.19	2.98E-07
Transcription	2.54	3.89E-07
Cellular protein complex assembly	10.31	4.54E-07
Chromatin modification	7.31	5.85E-07
Negative regulation of macromolecule metabolic process	4.10	1.03E-06
M phase	6.09	3.49E-06
Response to unfolded protein	16.47	3.73E-06
Cell cycle phase	5.24	5.28E-06
Macromolecular complex assembly	4.02	6.81E-06
DNA metabolic process	4.62	7.64E-06
Protein folding	8.49	9.53E-06
Protein import into nucleus	13.59	1.14E-05
Nuclear import	13.29	1.30E-05
Macromolecular complex subunit organization	3.76	1.49E-05
Protein localization in nucleus	12.44	1.90E-05
Nucleocytoplasmic transport	8.56	3.72E-05
Response to protein stimulus	10.93	3.98E-05
Nuclear transport	8.46	4.04E-05
Histone H2A acetylation	55.67	4.22E-05
Mitosis	6.83	4.57E-05
Nuclear division	6.83	4.57E-05
M phase of mitotic cell cycle	6.71	5.19E-05

Table 3.

Biological Processes Term	p-value
GO:0031145~anaphase-promoting complex-dependent proteasomal ubiquitin-dependent protein catabolic process	**1.69E-03**
APC1, CDK1, APC5, PSMA4, APC4, CDC23, UBC	
GO:0051169~nuclear transport	**6.65E-05**
NCBP1, MCM3AP, NUP160, RAN, IPO5, SPTBN1, NOP58, KPNA4, RANBP2, THOC2, KPNA2, KPNB1, KPNA1	
GO:0042254~ribosome biogenesis	**4.90E-06**
NPM1, LAS1L, NOP58, FBL, RPS2, PELP1, RPS4X, RPS5, RPS3, HEATR1, RPS8, RPS6, GEMIN4, RPS24, DDX21, TEX10, WDR18, WDR3, CCT3, BMS1, GEMIN5, RPS14, RPS16, RPS18, RPS27, RPL13, RPL18, NOP56, EIF4A3	

Table 4.